Flume Experiments on the Geometry of Local Scour Holes at Boulder-Like Obstructions during Unsteady Flow Conditions: Part II – Enlargement Processes and the Impact of Hydrograph Chronology

O. Schlömer[1], and J. Herget[1]

[1]Department of Geography, University of Bonn, Germany

Corresponding author: Oliver Schlömer (oschloem@uni-bonn.de)

Key Points:

- The enlargement of local scour hole length and width depends on scour hole depth rather than on actual flow conditions
- The size of local scour hole length and width in time can be estimated by an mechanistically model incorporating local scour depth
- For a hydrograph chronology the dependence on antecedent sizes of local scour depth, length, and width is important (memory effects)

This manuscript is the companion to:

Schlömer, O., & Herget, J. (2021): *Flume Experiments on the Geometry of Local Scour Holes at Boulder-Like Obstacles during unsteady flow conditions*: *Part I Hydrograph Shape and Intensity* (submitted to WRR)

Abstract

Local scouring is typically a bed load transport phenomenon that is well studied at bridge piers while less attention is given to the enlargement processes of local scour holes at natural instream obstacles like boulders. This specifically applies to changing hydraulic boundary conditions at the obstacle in the course of flood hydrographs while physical modelling in flumes offers the advantage that hydraulic boundary conditions can be systematically varied. This second companion paper yields novel experimental data on the role of hydrographs of different shape and flow intensity onto enlargement processes of local scour holes at boulder-like obstructions and evaluates the impact of hydrographs chronology on the local scour hole geometry. In total 48 unscaled process-focussed flume experiments at a range of flows (subcritical, clear-water and live-bed conditions) were performed. Experimental results revealed that (1) the enlargement of local scour hole length and width depends on scour hole depth rather than on actual flow conditions while an empirical model is presented that mechanistically predicts enlargement in local scour length and width based on (i) scour depth, (ii) the inclination of scour slopes and (iii) the planform area of the scour hole bottom. (2) In the course of subsequent hydrographs memory effects (i.e. the dependence on antecedent sizes of local scour depth, length, and width) have to be considered. This contribution improves the understanding of local scouring at boulder-like obstacles exposed to hydrographs while it is speculated that the identified memory effect may be utilized for hydraulic interpretation at field condition.

Plain Language Summary

Local scour holes are conical depressions related to instream obstructions like bridge piers or boulders that are exposed to flowing water. Scour holes emerge due vortices in the vicinity of the obstacle that mobilize sediment. Although the depth of local scour holes at bridge piers is well studied because of safety problems, there is scarce knowledge on the enlargement processes of the local scour hole in length and width at natural obstacles in rivers like boulders. This specifically applies to the importance of subsequent flood events onto the geometry of local scour holes.. However, the direct investigation of local scouring during floods is dangerous so that the phenomenon is investigated in flumes that simplify natural conditions. We present the results of a laboratory study on local scouring at boulder-like obstacles exposed to idealized floods of different shape, duration, and intensity and investigate the role of repeated floods. The results reveal that enlargement of local scour hole length and width depends on local scour depth rather than on actual flow conditions. Although local scouring is accumulating a dependence on antecedent sizes of local scour depth, length, and width is concluded, referred to as memory effects of the local scour hole.

1 Introduction

Local scour holes are conical depressions related to instream obstructions that result from three-dimensional vortices that induce sediment mobilization (Richardson, 1968; Allen 1984). Local scouring can occur for clear-water and live-bed conditions, which distinguishes presence and absence of general sediment mobilization in the undisturbed flow. For live-bed conditions the flow intensity (i.e. mean approach flow velocity relative to threshold velocity for general sediment movement) is greater than 1.

Technical infrastructure like bridge piers and abutments (Pizarro et al. 2020) as well as natural obstructions like solitary boulders with a diameter greater than the mean diameter of the surrounding alluvium can act as an obstacle. Thereby, local scour holes are consistent across spatial scales (10^{-2}m – 10^{1}m) while they are transient in the sense that they persist as long as the obstacle that creates them (Schlömer et al. 2021). A local scour hole can be characterized by certain length scales, including scour hole depth at the obstacle front (d_s) measured from the undisturbed upstream bed; scour hole frontal length (l_s) in the plane of symmetry to the incoming flow, measured from the obstacle frontal face to the upstream edge of the scour hole, and scour hole frontal width (w_s) measured perpendicular to the direction of incoming flow form the lateral edges of the scour hole at the obstacle frontal face (Figure 1a). The local scour hole has an elliptical shape in plan-view (w_s 2.5* l_s).

Research on local scouring relevant to different disciplines in Earth-science and hydraulic engineering while the phenomenon is predominantly investigated by scaled or unscaled physical modelling studies (Ettema et al. 1998). The applied engineering practice focuses on physical modelling to determine predictive equations for equilibrium d_s at technical infrastructure while neglecting l_s and

w_s. Equilibrium d_s is defined as maximum d_s that is reached asymptotically in time after a prolonged exposure to steady flow, typically in order of days for sand and gravel (Ettema et al. 2012). Therefore, physical modelling studies assume steady peak discharge over a theoretical infinitive duration (Manfreda et al. 2018). Although, equations are believed to be conservative (Sheppard et al. 2014), Tubaldi et al., (2017) pointed out that present experimental methodologies neglect two important characteristics that might lead to biased estimates of equilibrium scour depth: (1) natural floods are characterized by unsteady discharge (i.e. velocity and flow depth at any fixed point in space varying over time) expressed as hydrographs of different shape (i.e. time to peak discharge) which depends on rainfall intensity, catchment characteristics, and others (Rodríguez-Iturbe & Valdés 1979, Collischonn et al. 2017) that impact the evolution of local scouring; (2) local scouring is not independent from past events.

For (1), experimentally studies found that that the rising limb and peak flow have the strongest impact onto local scouring at bridge piers and time to reach maximum scour depth is reached usually smaller than the flood duration (Bombar 2020; Chang et al. 2004, Gjunsburgs et al. 2010, Tabarestani & Zarrati 2017).

For (2), it is assumed that scour depth at bridge piers is accumulating due to discharge chronologies with different flow intensity and hydrograph shape (Link et al. 2017; Pizarro & Tubaldi, 2019) which is referred as memory effect (Tubaldi et al. 2017).

However, at solitary boulders often used as measure in river restoration practices to enhance habitat quality (Shamloo et al. 2001), unsteady discharge even causes significantly different hydrodynamic conditions that result in emergent conditions during lower flows (some portion of the obstacle protrudes above the water surface) and submerged conditions at higher flows (the obstacle occupies only the lower portion of the flow) which is only scarcely addressed by experimental investigations (Euler et al. 2017).

Although, the spatio-temporal evolution of local scouring at boulder-like obstructions is experimentally modelled for long lasting steady discharge of different flow intensities (Schlömer 2020), no experimental data on the enlargement processes in d_s, w_s, and l_s during unsteady discharge and the impact of subsequent discharge events is available.

Thus, we experimentally investigate the impact of hydrographs of different shape, varying duration, and different intensity onto enlargement processes of local scouring at boulder-like obstacles and the effects of discharge chronologies. Within this context, the objective of the contribution is not to derive a predictive equation for local scouring during hydrographs, but to:

1. Analyze the enlargement processes of local scour holes for unsteady discharge in time by a systematic laboratory flume study.
2. Evaluate the history-dependence of local scouring at boulder-like obstruc-

tions for different hydrograph scenarios.

An improved understanding of the geometry of local scour holes in time can therefore be auxiliary to (a) refine existing procedures to estimate parameters (e.g. duration) of past flood events at field conditions (Herget et al. 2013) and (b) estimate the spatial extent of countermeasure for local scour protection at technical infrastructure.

The study is related to a companion that evaluates the impact of hydrograph shape and flow intensity onto the geometry of local scour holes and geometrical relations (i.e. d_s/l_s and d_s/w_s) at boulder-like obstructions (Schlömer& Herget, 2021). For both contributions a process-focused physical model approach was chosen that reproduces processes and resulting morphologies. The hydrographs were modelled upon dimensionless parameters, but do not represent a specific natural prototype.

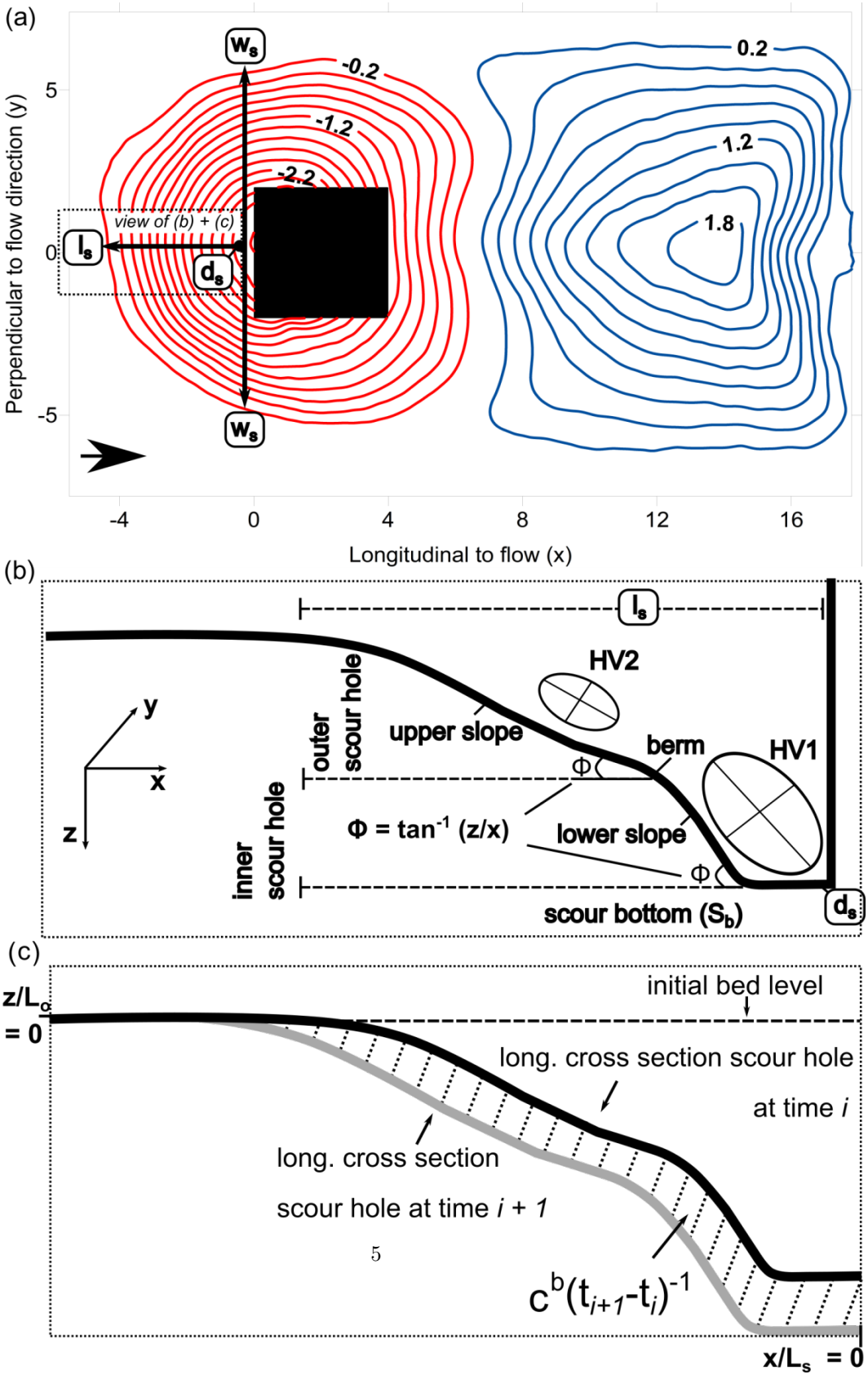
(a)
Perpendicular to flow direction (y)
Longitudinal to flow (x)
5
0
-5
-4
0
4
8
12
16
w_s
l_s
d_s
view of (b) + (c)
-0.2
-1.2
-2.2
0.2
1.2
1.8
(b)
l_s
HV2
HV1
upper slope
berm
outer scour hole
inner scour hole
lower slope
Φ
Φ = tan^{-1} (z/x)
y
x
z
scour bottom (S_b)
d_s
(c)
z/L_o = 0
initial bed level
long. cross section scour hole at time *i*
long. cross section scour hole at time *i + 1*
$c^b(t_{i+1}-t_i)^{-1}$
x/L_s = 0

Figure 1. (a) Plan view of an obstacle mark at a cube at laboratory scale (cm) defining characteristic morphometric variables of local scour hole (red isolines) and sediment ridge (blue isolines). Arrow indicates direction of flow. (b) Upstream cross-sectional profile of the local scour hole indicating internal differentiation and positions of primary horseshoe vortex (HV1) in back-flow mode, and secondary horseshoe vortex (HV2), (not to scale). (c) Definition of subsequent cross-sections for the estimation of the sediment transport rate (q^b) in non-dimensional form.

1. Boundary Conditions of Local Scouring at Natural Obstacles

Local scouring is the result of a complex two-phase flow involving water and sediment (Radice et al. 2009), that is controlled by different extrinsic and intrinsic environmental boundary conditions comprising (1) flow conditions, (2) sediment characteristics, (3) properties of the obstacle, and (4) time (Breusers & Raudkivi 1991; Melville & Coleman 2000)

Local scour incision at a solitary boulder-like obstacle located in a straight, moderately sloped channel and embedded in non-cohesive sediment functionally depends on a set of dimensionless control parameters (Schlömer et al. 2020):

$$d_s/L_o = f\,(d_w/L_o,\ U_m/U_c,\ Re_o,\ L_o/B,\ Sh,\ Mb,\ L_o/D_{50},\ _G,\ d_{sed}/L_o,\ t/t_e) \quad (1)$$

where d_w/L_o is the submergence ratio (d_w = flow depth [L] and L_o = effective obstacle size ${h_o}^{2/3}\ {w_o}^{1/3}$ [L], with h_o = obstacle height [L] and w_o = obstacle width [L], U_m/U_c is flow intensity (U_m = mean approach velocity [LT^{-1}] and U_c = critical mean approach velocity for entrainment of sediment [LT^{-1}]), Re_o is the obstacle Reynolds number ($U_mL_o/$, with = kinematic viscosity of water [L^2T^{-1}), L_o/B is the blockage ratio (with B = channel width [L]), Sh [-] is an indicator for the hydrodynamic shape of the obstacle, Mb [-] is an indicator for the mobility of boulder-like obstruction due to tilting into the local scour hole, L_o/D_{50} is the relative sediment coarseness (D_{50} = median diameter of the bed sediment [L]), $_G$ is the sorting of sediment (${D_{84}/D_{16}}^{1/2}$ [-]), d_{sed}/L_o is the relative thickness of the alluvial layer (d_{sed} = thickness of the alluvial layer in which the obstacle is embedded [L]), and t/t_e is the time scale of local scouring.

Hence, laboratory investigation of local scouring in a physical model (i.e. flume) offers the advantage that boundary conditions can be varied systematically while each term in Eq. (1) is measurable or readily simulated with the current state-of-the-art technology for measuring or time-dependent riverbed elevation evolution.

1.2 Processes of Local Scouring

Local scouring originates from a deformations of the approaching flow field in the vicinity of an obstacle that cause (1) contradiction of streamlines lateral to the obstacle, inducing higher flow velocities; (2) formation of a jet-like downflow at the obstacle front due to pressure gradient; (3) formation of unsteady turbulent necklace-like vortical structures at the obstacle base commonly referred as horseshoe vortex system (HV) (Escauriaza & Sotiropoulos 2011; Kirkil & Constantinescu 2010; Radice & Tran 2012). Processes (1) to (3) amplify bed

shear stress by one order of magnitude larger than those generated by classical turbulent shear mechanism in the approach flow inducing sediment mobilization even if sediment transport in the undisturbed approaching flow is absent and clear-water conditions prevail ($U_m/U_c < 1$) (Li et al. 2018; Link et al. 2012). Typically, scouring starts at the lateral edges of the obstacle perpendicular to current direction and forms two depressions that merge to an initial local scour hole in front of the obstacle (Dargahi, 1990). Within this initial scour hole the HV actually consists of several interacting and unsteady vortices (Kirkil et al., 2008; Chen et al., 2017). The largest and most stable vortex is denoted as the primary horseshoe vortex (HV1) and is located close to the obstacle base while upstream, a smaller and less coherent vortex (HV2) is located within the outer region of the frontal scour hole. The presence of different vortices is evident by considering a longitudinal profile from the obstacle frontal face to the upstream edge of the scour hole where a segmentation of the local scour hole slope is obvious. These segments consist of: (1) a flat semi-circular scour hole bottom (S_b) that is closely attached to the obstacle base with radius $< l_s$, (2) an inner frontal scour hole (lower slope) that is characterized by an inclination (Φ) critical angle of repose (Φ_{crit}), and (3) an outer frontal scour hole (upper slope) that is characterised by Φ Φ_{crit}. The transition between both slopes is marked by a knickpoint (berm) in the cross-sectional profile (Figure 1b).

The steeper inner scour hole is shaped by the rotation of the HV1 that generally stabilizes the lower slope in an angle greater than the angle of repose (Bateman et al. 2006). However, the HV is an unsteady vortex system that randomly oscillates in time, and thereby temporarily weakens due to aperiodic bimodal oscillations that cause changes in the position and shape of the vortex core from circular (zero-flow mode) and closely aligned to the obstacle, to elliptical (back-flow mode), where the core is situated away from the obstacle (Paik et al., 2007; Kirkil and Constantinescu, 2015). In back flow mode, the vertical extent of HV1 coincides with the knickpoint in the slopes, differentiating the outer and inner frontal scour hole (Muzzammil and Gangadhariah, 2003; Unger and Hager, 2007).

During incision HV1 sinks into the frontal scour hole and extends down to S_b. The non-linear depth-incision in time is caused due to an expansion of the HV diameter that decreases the shear stress beneath the vortices and induces an equilibrium condition if the HV is no longer capable of removing sediment (Kothyari et al. 1992). From laboratory data at clear-water conditions it is well established that 80% of equilibrium d_s is developed within only 5-40% of the time to equilibrium that is obtained after several days, mainly depending on approach flow velocity (Melville & Chiew 1999). The enlargement of l_s and w_s is related to depth incision and occasionally weakening of the HV that destabilizes the scour slopes and results in gravity mass movements. The sediment grains slide into S_b where they get picked up by the HV1 and are transported downstream under its expanding legs as bed load.

For experiments on long lasting constant discharge Schlömer et al., (2021) for-

mulated a quantitative model that mechanistically predicts enlargement in l_s and w_s based on (1) d_s, (2) Φ, and (3) S_b. However, the consistency of the model at unsteady discharge and discharge chronologies is unevaluated yet.

2. Experimental Design

2.1 Flume Set-Up

Physical modelling was conducted in a in a 5 m long, 0.32 m wide, and 0.27 m deep straight rectangular flume with fixed slope (0.003 m m^{-1}) entirely filled with a 5.5 cm thick layer (d_{sed}) of uniform ($_G < 1.3$) sand with median grain diameter (D_{50} = 0.75 mm). D_{16} and D_{84} were 0.61 mm and 0.89 mm, respectively. The critical angle of repose (Φ_{crit}) when dry is estimated ~ 33° (Dey 2014). Discharge was controlled by a recirculating pump (Lowara FCE-series®) regulated by two cone valves and measured by a magnetic-inductive discharge meter (Schwing MS 1000®, accuracy ± 1% of actual discharge). Flow depth (d_w) was adjusted by a tail-gate at the downstream end of the flume to enable pseudo-uniform flow (Hager & Hutter 1984) within the working section of the flume (~ 2.7 m downstream of the inlet). The water surface profile was measured using an ultrasonic distance meter (Mic +25, Microsonic®, accuracy ± 0.1 mm). A cube (L_o = 3 cm) was used to mimic an angular instream boulder-like obstacle that was mounted to the flume bottom within the working section to prevent tilting. The obstacle was placed in the working section of the flume in the plane of symmetry to minimize sidewall effects (Nakagawa and Nezu, 1993). Blockage ratio (L_o/B, with B = flume width) and relative sediment coarseness (L_o/D_{50}) were designed to satisfy critical thresholds for the onset of local scouring, i.e. $L_o/D_{50} > 8$ (Lee and Sturm, 2009), and L_o/B < 0.6 (Williams et al., 2019).

2.2 Test Program

Laboratory hydrographs were modelled upon the principle of stepped hydrographs i.e. sequences of constant discharges acting during defined intervals which is commonly used to simulate varying discharge in flumes (Link et al. 2017; López et al. 2014; Mao 2012). The stepped hydrographs were constructed with 13 intervals of constant discharge: six on the rising limb, one at peak flow, and six on the falling limb for three experimental series (A, B, C) that had different overall durations (t_e). For series A the experimental duration (t_e) was 480 min, for series B t_e was 210 min, and for series C t_e was 120 min.

For each experimental series the duration of rising limb (t_r), falling limb (t_f), and peak flow (t_{peak}) was variable to generate four, relatively simple shaped single peaked hydrographs (i.e. symmetrical (t_r/t_f = 1), positive skewed (t_r/t_f < 1), negative skewed ($t_r/t_f > 1$), and flash flood hydrograph (t_r/t_f « 1)) (Figure 2a-d) while details on the construction of the hydrographs are given in Schlömer and Herget (2021). Different unit discharges (q) on each interval were generated by a variation of d_w and U_m (Table 1). The hydrographs started from a drained flume (i.e. no baseflow) and d_w was linearly increased up to peak flow (q_p) and then was linearly decreased again, producing emergent (d_w/L_o < 1)

and submerged conditions (d_w/L_o » 1) at the obstacle during the hydrographs. Different flow intensities (U_m/U_c) were created that distinguish between clear-water conditions (U_m/U_c 1, scenario 1 and 2), as well as live-bed conditions (U_m/U_c >1.01, scenario 3) for each hydrograph shape. Details on the estimation of U_c for different d_w is provided in Schlömer and Herget (2021).

The hydrographs were also operationalized by calculating the dimensionless total flow work index, W_k as indicator for the magnitude (Waters & Curran 2015)

$W_k = u_p{}^{*2} /(g d_w{}^3 B)$ (2)

where $u_p{}^*$ is the shear velocity [LT^{-1}] at peak flow (q_p), is the total volume of water under the hydrograph [L^3], and g is gravitational acceleration [LT^{-2}]

$u_p{}^*$ was estimated from semi-logarithmic velocity profiles (Bergeron & Abrahams 1992) measured from an acoustic Doppler velocimeter (ADV), yielding $W_k = 1.70$ for scenario 1, $W_k = 2.46$ for scenario 2, and $W_k = 3.49$ for scenario 3. For scenario 3, sediment was solely transported as bed load (i.e. lower stage plane bed). In total 36 experimental runs were performed.

The impact of hydrograph chronologies (i.e. sequences of hydrographs with a certain shape) onto local scouring was evaluated in a second experimental campaign by repeating the positive, negative and flash-flood hydrograph for series C at $W_k = 1.70$ (i.e. C4, C7, and C10; $t_e = 120$ min) three times in a row (Figure 2e-g, i.e. flood I-IV). Therefore, for a specific hydrograph the overall experimental duration equaled 480 min while 12 additional experimental runs. were performed.

Table 1. Hydraulic boundary conditions of experimental series

	Scen. 1[a, d] W_k = 1.70	Scen. 2[b] W_k = 2.46	Scen. 3[c] W_k = 3.49					
Interval (n) [-]	d_w [m]	U_c [ms^{-1}]	U_m [ms^{-1}]	q [m^2s^{-1}]	U_m [ms^{-1}]	q [m^2s^{-1}]	U_m [ms^{-1}]	q [m^2s^{-1}]
+ 13				10^{-5}		10^{-5}		10^{-5}
+ 12				10^{-5}		10^{-5}		10^{-5}
+ 11				10^{-5}		10^{-5}		10^{-4}
+ 10				10^{-4}		10^{-4}		10^{-4}
+ 9				10^{-4}		10^{-4}		10^{-4}
+ 8				10^{-4}		10^{-4}		10^{-4}
				10^{-4}		10^{-4}		10^{-4}

Note. [a] A/B/C 1, 4, 7, 10. [b] A/B/C 2, 5, 8, 11. [c] A/B/C 3, 6, 9, 12. [d]C 4, 7, 10 were used to model subsequent hydrographs.

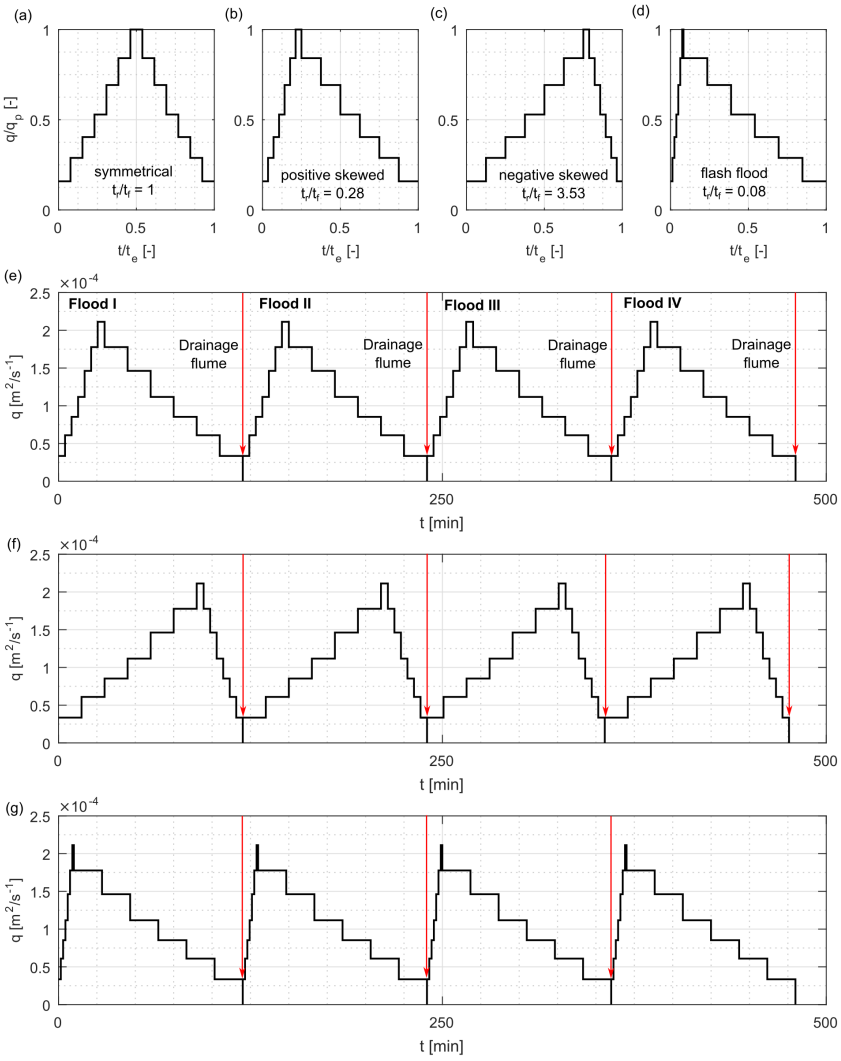

Figure 2. Laboratory hydrographs for series A, B, and C (a-d) and principle of subsequent hydrographs for C4 (e), C7 (f), and C10 (g)

2.3. Working hypotheses

By neglecting constant boundary conditions of the experiments ($L_o/B = 0.09$, $L_o/D_{50} = 40$, $_G < 1.3$), and neglecting viscous effects (Manes et al. 2018) equation (1) reduces to

$$d_s/L_o = f\,(d_w/L_o,\ U_m/U_c,\ t/t_e) \quad \ldots(3)$$

where t_e is interpreted as the overall duration of laboratory hydrograph while

each hydraulic parameter in equation 1 is of particular interest for modelling varying discharge in course of a hydrograph and evaluating its impact on processes of local scouring. Within this context, it is worthwhile to mention that neither hydrographs nor obstacle dimensions were scaled to a prototype and the flume experiments are interpreted as unscaled process-focused physical models (Baynes et al. 2018).

By assuming shape similitude of the local scour hole (cf. Chreties et al. 2008), non-dimensional scour depth (d_s/L_o) in equation 3 can be replaced by non-dimensional scour length (l_s/L_o) or non-dimensional scour width (w_s/L_o). However, it is hypothesized that for given sediment size and obstacle size, l_s/L_o and w_s/L_o scale with d_s/L_o and elapsed time, and only indirectly with the actual flow conditions. Thus, the working hypotheses is:

1. The dimensions of l_s/L_o and w_s/L_o in time are dependent on d_s/L_o and essentially unaffected by flow conditions which reduces equation (3):

l_s/L_o, w_s/L_o = f (d_s/L_o, t/t_e) (4)

1. In the course of discharge chronologies it is hypothesized that subsequent hydrograph events will cumulate d_s/L_o over time while l_s/L_o and w_s/L_o scale with d_s/L_o.

2.4 Experimental Procedure

For each experimental series the experiments started at t = 0 min after adjusting d_w and q to the first interval of the hydrograph and introducing the obstacle in the working section to induce local scouring immediately. Between intervals on the rising limb the tailgate was raised 1 to 2 cm to interrupt local scouring while q was adjusted to the next interval. On the falling limb, first q was decreased while the tailgate was lowered to the corresponding d_w.

During the experimental campaign on flood sequences of C4, C7, and C10 the pump was stopped after individual hydrographs (i.e. t = 120 min) and the flume was carefully drained. Afterwards, the flume was filled again to d_w = 2 cm before the pump was started at q of the first hydrograph step. It is worth mentioning that the procedure did not cause distortions of the local scour hole (i.e. collapsing of local scour hole flanks).

2.5 Data Acquisition and Processing

Dimensions of d_s, l_s, and w_s were measured with two LED-distance meters (Welotec® OWRB-series, accuracy ± 0.5 mm), measuring x- and y-coordinates in a local Cartesian coordinate system, with x = longitudinal, streamwise direction and y = lateral, perpendicular to streamwise direction; and a laser distance meter (Baumer Electric® ODAM S14C, accuracy ± 1.5 mm) measuring the vertical coordinate (z). The sensors were mounted on a cart on top of the flume operating in x/y –plane. The elevation of the initial flat bed in front of the obstacle was used as reference (i.e. x/y/z = 0/0/0).

For series A measurements of d_s, l_s, and w_s were sampled every third minute on each hydrograph step. For series B and C the measurement frequency was relaxed to one and two min, respectively, to generate sufficient data on each hydrograph step.

Measurements of morphometric variables are interpreted as quasi-dynamic observations, because they were measured while water was flowing (Rogers et al., 2020). Measurements of the z-coordinate were biased due to refraction of the laser beam within the water column. However, a simple calibration method (i.e. compensation for the travel time of light in water) yielded sufficiently accurate results when compared to measurements at drained conditions with the same measurement system (Schlömer et al. 2021). Additionally, the geometry of the local scour hole was measured by 2D cross-sectional profiles in the longitudinal and lateral directions according to the definition in Figure 1a (solid lines). Profiles were surveyed every 20 minutes up to t_e of the experimental series. Two consecutive frontal scour profiles were used to estimate the volumetric bed load transport rate (q^b [L^2T^{-1}]) out of the frontal scour in absence of sediment suspension by calculating the line integral (Figure 1c):

$$q^b \ (l_{sP} \ v \ w_{sP}, \ t) \quad c^b/t_{(i+1)} - t_{(i)} \ (5)$$

with l_{sP} = longitudinal scour hole profile or w_{sP} = lateral scour hole profile, c^b = depth-integrated frontal scour hole area, and i = 1, …N in which N is the total number of measured profiles in time.

For comparison, frontal scour hole profiles were scaled with the corresponding dimensions of d_s, l_s and $w_{s,}$ in order to preserve collinearity of distances and angles (i.e. three or more points initially lying on a line still lie on a line after the transformation) (Tregnaghi et al. 2017) while q^b was replaced by the dimensionless bed load q* [-]:

$$q^* = q^b/((\ s/\ -1)\ gD_{50}{}^3)^{1/2} \ (6)$$

with = water density [ML^{-3}] and $_s$ = sediment density [ML^{-3}].

For the experimental campaign on hydrograph sequences, the resulting morphology after each hydrograph at drained conditions was modelled by Structure-from-Motion Multi-View Stereo photogrammetry (SfM-MVS) (Smith et al. 2016, Morgan et al. 2017) to derive digital elevation models (DEMs) and quantify geomorphic changes caused due subsequent flood events by DEMs of difference (DoDs) (Wheaton et al. 2010). SfM-MVS operates as automated photogrammetry that can resolve 3-D structure from overlapping images taken from varying viewpoints (i.e. camera positions) (Westoby et al. 2012).

Images were acquired using a Panasonic Lumix DMC-G5 (DSLM) camera with a 4/3" (17.3 x 13.0 mm), 16 megapixel image sensor and a Lumix G-Vario 14-42 mm zoom lens set at 21 mm focal length for minimal image distortion (35 mm full frame equivalent) (Javernick et al. 2014, James et al. 2019) capturing images at 4608 x 3072 pixel size at 52° field of view. The camera was mounted on a

cart ~60 cm above the flume which corresponds to a ground sampling distance of 0.1 mm/pixel. By moving the cart along the longitudinal and lateral axis of the flume nadir imagery (i.e. pointing below a particular direction) were captured at 80% side and forward overlap over the area of interest (~ 30 x 50 cm). Additionally, images at an oblique angle (~ 45° off-nadir) were taken to enhance capturing steep features of the morphology (i.e. local scour hole). After each hydrograph a complete data set consisted of 95 images captured in 10 min. Prior to taking images, 8 Ground Control Points (GCPs) were distributed throughout the area of interest that consisted of coded circles with 4 cm diameter (Agisoft 2016). Target centroids were measured with measurement technique described above to obtain xyz coordinates.

For the processing PhotoScan software (version 1.2.6) (Agisoft 2016) was utilized. The SfM-MVS workflow is an iterative process comprised of (i) photo alignment using a point matching algorithm that detects key points in overlapping images and solves for camera position and camera lens parameters; the alignment accuracy was set 'high' and pair selection was disabled (key point limit 40000, tie point limit 1000), identifying > 1500 key points in each photoset; (ii) georeferencing based on 2/3 of the GCPs (the remaining GCPs were used for accuracy assessment) that optimized alignment and refined camera locations by minimizing the error between modeled locations and measured locations; according to Lane et al., (2000) and James et al., (2019) the mean error (ME) was used to estimate accuracy, mean absolute error (MAE) to estimate non-directional height differences, and standard deviations (SD) to estimate precision, yielding ME = -0.003 m (x-axis), -0.001 m (y-axis), 0.001 m (z-axis); MAE = 0.005 m (x-axis), 0.003 m (y-axis), 0.0007 m (z-axis); and SD = 0.009 m (x-axis), 0.004 m (y-axis), -0.001 m (z-axis); (iii) modelling of dense point clouds based on camera locations and Multi-View Stereo reconstruction, generating dense clouds with > $8*10^6$ points for each dataset; (iv) DEM generation based on dense point clouds at 0.2 mm/pixel (sub grain size) resolution for the each dataset to enable comparison.

DoDs were generated using Geomorphic Change Detection software (version 7) (Wheaton et al. 2010). Thresholds of change detection (i.e. levels of detection, LoD) to evaluate uncertainty were evaluated using standard Gaussian error propagation:

$$\mathrm{LoD} = ((\ (\mathrm{z})_{\mathrm{DEM\ t1}})^2 + (\ (\mathrm{z})_{\mathrm{DEM\ t2}})^2)^{1/2} \quad (7)$$

where $(\mathrm{z})_{\mathrm{DEM\ t1}}$ is the vertical error at time step 1, and $(\mathrm{z})_{\mathrm{DEM\ t2}}$ is the vertical error at time step 2, respectively. Areas below LoD were considered as noise, and areas above were interpreted as topographic changes.

3. Results

The experimental dataset is accessible via the Havard dataverse repository:

https://doi.org/10.7910/DVN/EYQP2U.

3.1 Local Scour Hole Geometry in Time´

For every experimental series two initial depressions formed at the lateral edges of the obstacle at t 0.1 min that rapidly merged to a conical local scour hole in front of the obstacle (t 1 min). The eroded material was deposited downstream in the wake of the obstruction as a sediment ridge with orientation parallel to the flow direction. Subsequently, the frontal scour hole deepened as well as lengthened and widened, while the sediment ridge flattened, widened and elongated in downstream direction. By neglecting different hydrograph shape (t_r/t_f) and duration (t/t_e) a monotonic increase and co-variation of l_s/L_o and w_s/L_o with increasing d_s/L_o is obvious (Figure 3a-f). The trend was present irrespective of hydraulic conditions for clear water (i.e. $W_k = 1.70$ and 2.46) and live-bed conditions ($W_k = 3.49$) during hydrographs while sizes of geometrical length scales scaled with W_k.

The conical shape of the local scour hole remained throughout the experiments as evident by the scaled longitudinal and lateral profiles of the local scour hole that superimposed and collapsed into a narrow band, irrespective of W_k, t/t_e and t_r/t_f (Figure 4). Additionally, the segmentation of the local scour hole was obvious irrespective of time (cf. Figure 4a-d and Figure 1b). However, considering an individual hydrograph shape the extent of S_b expanded from S_b/L_o 0.3 for t/t_e 0.25 to S_b/L_o 0.6 for $t/t_e > 0.5$ 1 while Φ of the upper scour hole slope showed a decreasing tendency, ranging from 32°-40° for t/t_e 0.25 and 23° to 32 for $t/t_e > 0.5$ 1.

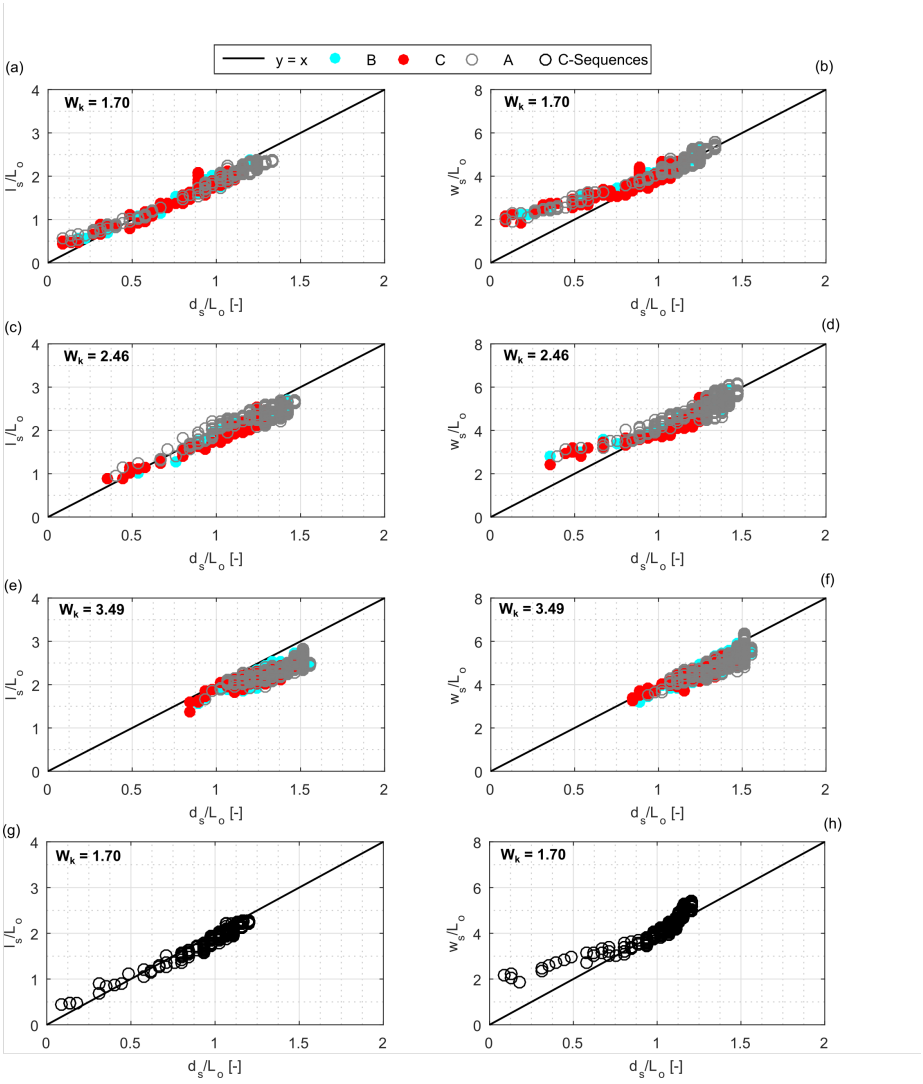

Figure 3. Relationship of non-dimensional morphometric variables for different W_k of experimental series A, B, and C.

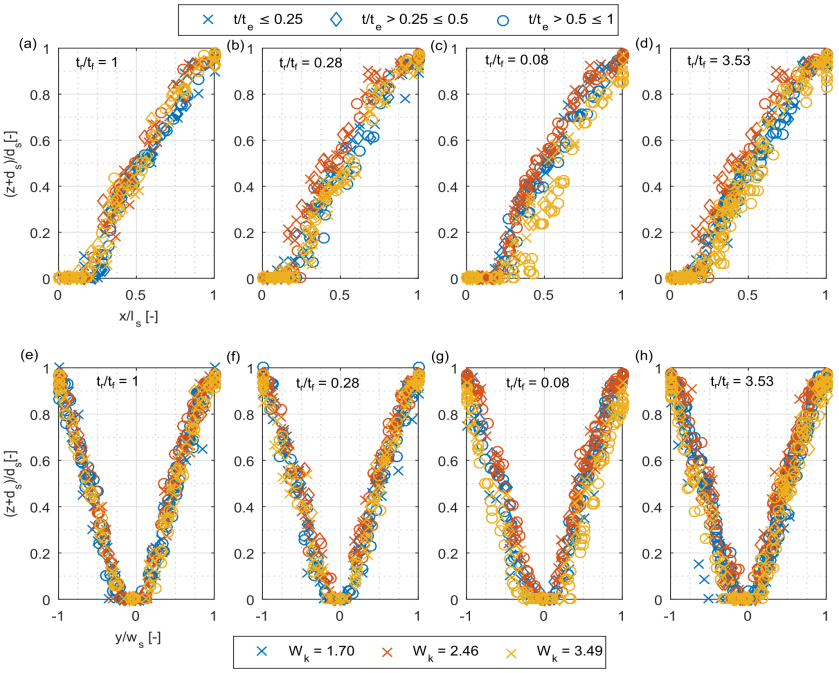

Figure 4. Scaled longitudinal profiles (a-d) and lateral profiles (e-h) of the local scour hole for different W_k and hydrograph shape

3.2 Bed Load Transport out of the Local Scour Hole

The estimated q* from longitudinal and lateral scour hole profiles showed an asymptotical behavior in time indicated by high q* at the beginning of experimental runs (i.e. t_r) due to strong depth-incision and simultaneous enlargement in l_s and w_s while q* significantly decreased proceeding q_p (Figure 5, vertical lines) and reached an almost null value on t_f. Neglecting different hydrograph shapes the trend could be approximated by a power law relationship and ordinary least squares estimation with a mean coefficient of determination (R^2) equaling 0.83 while for individual runs R^2 was considerable higher ($R^2 = 0.99$)

However, for live-bed conditions ($W_k = 3.49$, Figure 5 e, f) and irrespective of t_r/t_f q* turned negative approaching peak discharge as bed load sheets were transported into the frontal scour hole that reduced the spatial extent (in d_s, l_s, w_s) of the frontal scour hole between subsequent profiles. Afterwards, q* turns positive again, recovering to bed load comparable to q* prior to q_p which coincides with observations on slight enlargement of the local scour hole on the falling limb past to the refilling event (cf. Schlömer & Herget 2021).

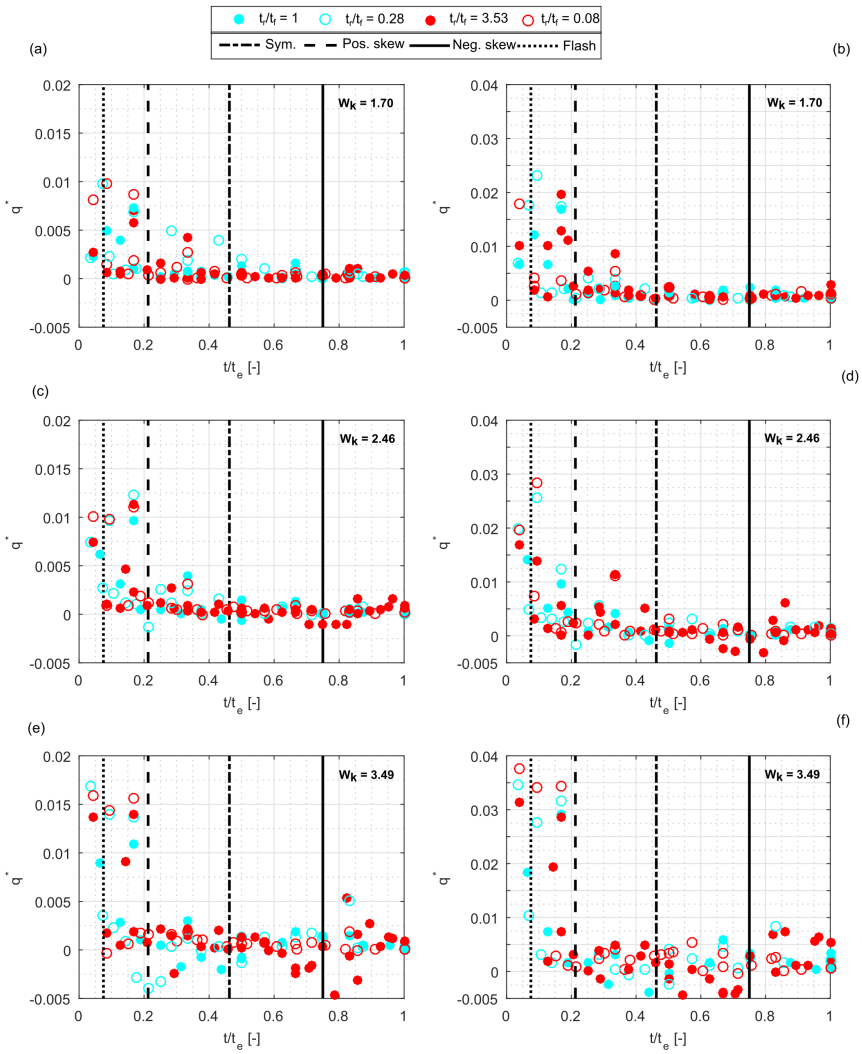

Figure 5. q* from longitudinal profiles (a, c, e) and lateral profiles (b, d, f) for different W_k and hydrograph shapes. Vertical lines represent the onset of peak discharge (q_p) for different hydrograph shapes

For further statistical analysis q* and t/t_e were log-transformed to derive linear relationships and an ANCOVA test (F-value = 1.32 – 1.59, p-value = 0.02 for longitudinal profiles; F-value = 1.28 – 1.32, p-value = 0.15 for lateral profiles) revealed that q* over t/t_e were statistically not different for different hydrograph shapes at 95% confidence interval.

3.3 Impact of Discharge Chronologies

Irrespective of hydrograph shape d_s, l_s, and w_s did increase from hydrograph

I to IV while a monotonic increase and co-variation of l_s/L_o and w_s/L_o with increasing d_s/L_o was present (Figure 3g-h). The modelled DEMs after each hydrograph showed that the local scour hole was persistent and enlarging with subsequent hydrograph events (exemplified for C10 in Figure 6a-d). However, DoDs could be constructed for a LoD = 0.1 cm (equation 7) and showed that the elevation change in between the hydrograph events were not equal (Figure 6e-g). Considerable erosion of the entire area of the local scour hole is present for DoD 1 while the amount is decreasing for DoD 2. For DoD 3 deposition is dominant due to the sediment reworking at the sediment ridge which extended in downstream direction.

The size of the local scour hole after hydrograph IV (d_{se}, l_{se}, w_{se} at t_e = 480 min) was equal to the size of d_s, l_s, and w_s of series A experiments with equal experimental duration (cf. Schlömer & Herget 2021).

Considering the entire history; d_s, l_s, and w_s did not increase linear as shown in Figure 6a-i. The increment of d_s and l_s was largest for the rinsing limb of event I (cf. vertical line Figure 7a-f) for which 80-90 % of the dimensions at t_e were reached. After hydrograph II substantial increment of d_s and l_s was negligible and asymptotically approached its final value at t_e = 480 min irrespective of hydrograph shape. However, slight enlargement of w_s was present past hydrograph II for all considered hydrograph shapes (Figure 7g-h). Thus, the geometrical relation of the local scour hole (i.e. d_s/l_s, d_s/w_s) over non-dimensional time are compose of a piecewise pattern composed of (a) considerable enlargement in d_s/l_s and d_s/w_s for event I and II as d_s increased quicker than l_s and w_s, approaching a maximum value in d_s/l_s and d_s/w_s at t/te = 0.04 (Figure 6j,k); (b) as scour incision relaxed and d_s matured to its finale size while slight enlargement in w_s occurred. Quantitatively, the stages are separated by change points that mark instabilities in the slope coefficients (ß1, ß2) for the regression of d_s/l_s and d_s/w_s over t/t_e (cf. Schlömer & Herget 2021).

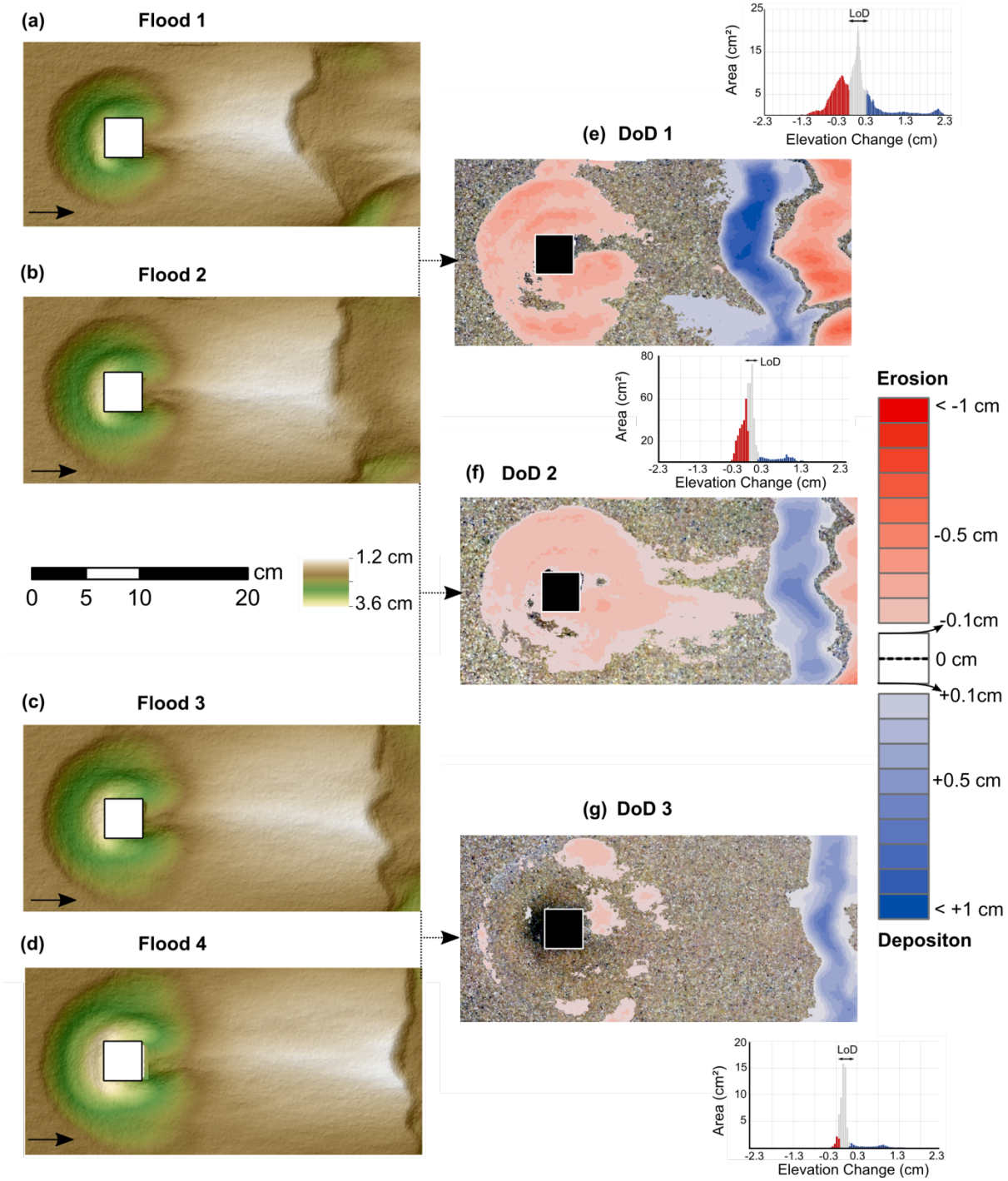
(a) Flood 1
(b) Flood 2
(c) Flood 3
(d) Flood 4
cm
0 5 10 20
1.2 cm
3.6 cm
(e) DoD 1
(f) DoD 2
(g) DoD 3
LoD
Area (cm²)
Elevation Change (cm)
Erosion
< -1 cm
-0.5 cm
-0.1cm
0 cm
+0.1cm
+0.5 cm
< +1 cm
Depositon

Figure 6. Modelled DEMs (a-d) and associated DoDs (e-g) for C10 hydrographs

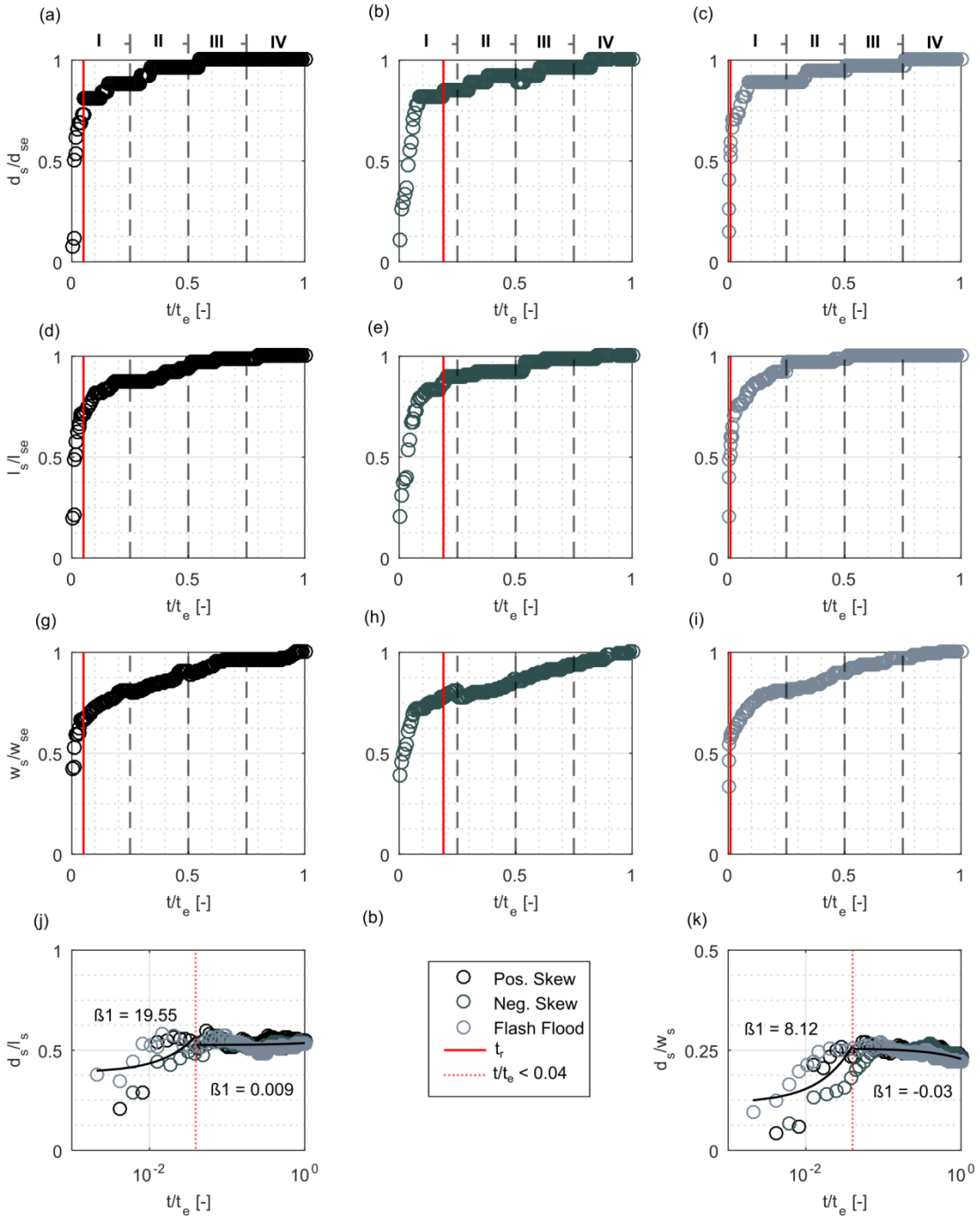
(a)
(b)
(c)
(d)
(e)
(f)
(g)
(h)
(i)
(j)
(b)
(k)
I
II
III
IV
d_s/d_{se}
l_s/l_{se}
w_s/w_{se}
d_s/l_s
d_s/w_s
t/t_e [-]
Pos. Skew
Neg. Skew
Flash Flood
t_r
$t/t_e < 0.04$
ß1 = 19.55
ß1 = 0.009
ß1 = 8.12
ß1 = -0.03

Figure 7. Trajectory of d_s, l_s, and w_s evolution for subsequent hydrograph events (W_k = 1.70) (a-i) and geometrical relations over non-dimensional time scale (j,k)

3.4 Model of Local Scour Hole Enlargement

Two mechanistically models are proposed to assess the enlargement of l_s and w_s in time based on (i) d_s, (ii) cotangent of slope inclination ($\tan^{-1}$ (Φ)), and (iii) the span of the scour hole bottom (S_b). The models were constructed upon data of all experimental series (W_k = 1.70 – 3.49) neglecting different hydrograph shapes using bootstrapped regression for insensitivity to outliers (Davison and Hinkley, 2009).

According to Figure 8a, l_s/L_o can be estimated by:

$l_s/L_o = 1.26*(d_s/L_o*\cot\ \Phi+S_b)$ (8)

The analysis of w_s in regard to (i), (ii), and (iii) is complemented by the constant 2 due to the relationship of l_s to w_s (Schlömer et al. 2021) (Figure 8b):

$w_s/L_o = 2{,}72*(2*d_s/L_o*\cot\ \Phi+S_b)$ (9)

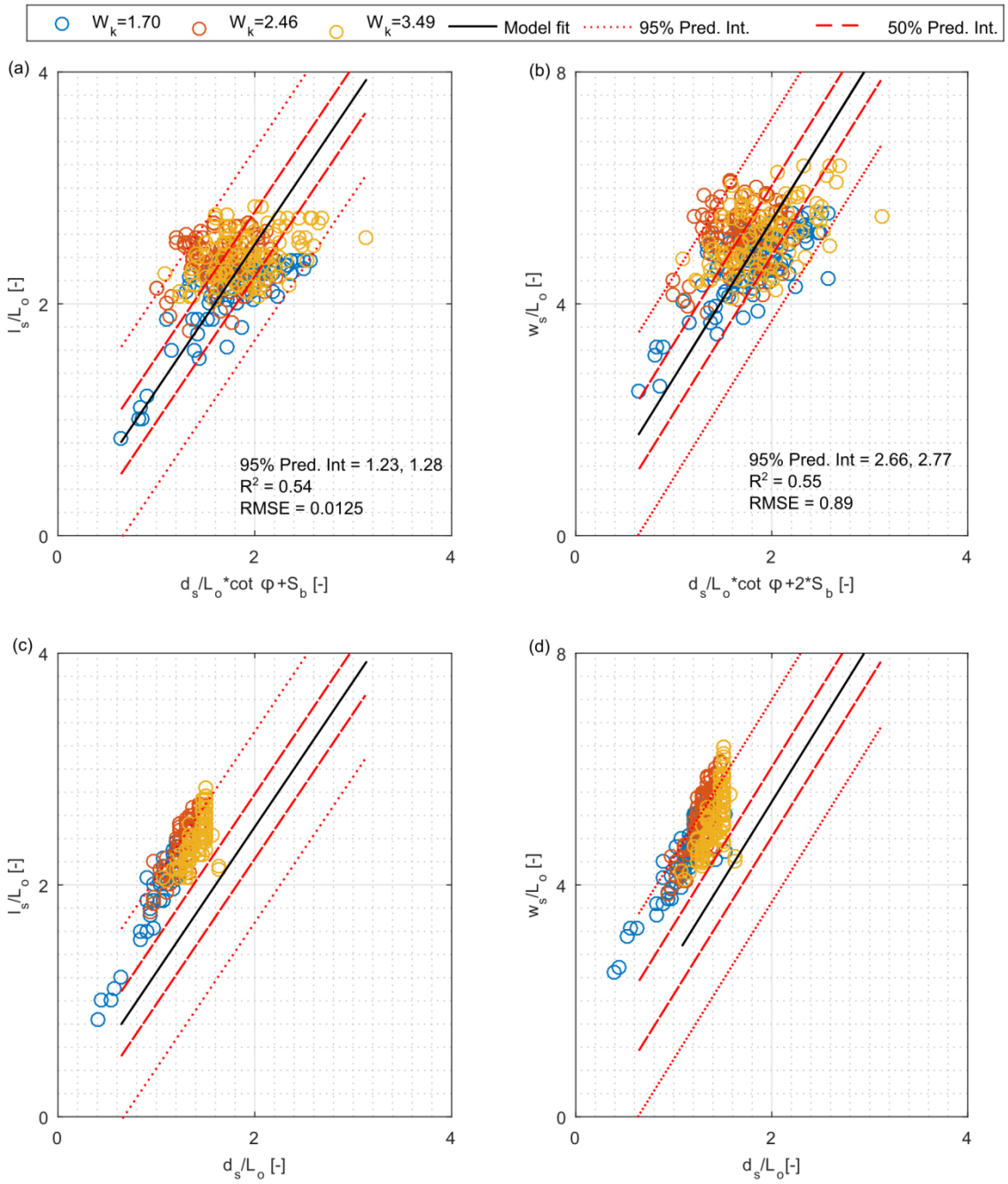
W_k=1.70
W_k=2.46
W_k=3.49
Model fit
95% Pred. Int.
50% Pred. Int.
(a)
l_s/L_o [-]
d_s/L_o*cot φ+S_b [-]
95% Pred. Int = 1.23, 1.28
R^2 = 0.54
RMSE = 0.0125
(b)
w_s/L_o [-]
d_s/L_o*cot φ+2*S_b [-]
95% Pred. Int = 2.66, 2.77
R^2 = 0.55
RMSE = 0.89
(c)
l_s/L_o [-]
d_s/L_o [-]
(d)
w_s/L_o [-]
d_s/L_o[-]

Figure 8. Model of local scour hole enlargement in l_s/L_o and w_s/L_o (a,b) and experimental observations (c,d)

4. Interpretation and Discussion

4.1 Local Scour Hole Enlargement

Experimental results support working hypothesis (a). Local scour incision is triggered by the HV that sinks into the emerging scour hole and expands its diameter indicated by an expansion of S_b with d_s and t. The expansion decreases the shear stress beneath the vortex for sediment mobilization and induces equilibrium of depth-incision (Dargahi 1990; Unger & Hager 2007). Thus, local scour hole and HV system in time are connected via feedback loops indicating a self-organizing behavior (Coco & Murray 2007).

The enlargement of l_s and w_s is directly coupled to d_s as the local scour incision undermines the local scour slopes and induces gravitational movements at the flanks, indicated by slope angels that adjust to the critical angle of repose (Φ_{crit}).

As shown in Figure 8c, d, the experimental observations on l_s/L_o and w_s/L_o were larger than the model estimations, nevertheless they indicate reasonable agreement within the prediction bounds (Figure 8c-d). However, similar mechanistically models of local scour hole enlargement are presented in Schlömer et al., (2021) on experimental data a steady discharge and in situ field evidence of local scour holes at boulders in the Colorado River while the dependency of the geometrical length scales of the local scour hole on each other is also reported by physical modelling studies on local scouring at bridge piers (Bateman et al. 2006; Chreties et al. 2008; Chreties et al. 2013).

4.2 Bed Load Transport and Local Scour Hole History

For individual hydrographs, the estimated bed load transport rates (q^b) out of the local scour hole varied at the same unit discharge (q) on t_r and t_f which is referred as hysteresis (Brownlie 1981). For clear-water conditions (W_k = 1.70) the bed load transport exhibited a clockwise hysteresis pattern irrespective of hydrograph shape (Figure 9a, d, g, j). The high transported rated at the beginning stages of t_r are forced due to the for relatively shallow flow conditions in which flow depth was comparable to the obstacle size (i.e. $d_w/L_o = 1$). At this, an intense downflow at the obstacle front and an efficient HV system at the base persist. With increasing q and vice versa increasing d_w/L_o this physical effect weakens as the obstacle becomes submerged ($d_w/L_o > 1.1$) (Schlömer et al. 2020). Thus, bed load out of the local scour hole diminishes approaching q_p. For W_k = 2.46 (i.e. close to general bed load mobilization $U_m/U_c > 1$, cf. Table 1) and W_k = 3.46 (live-bed conditions) a figure-8 hysteresis loop (Williams 1989) was present for the symmetrical, positive skewed, and negative skewed hydrographs (Figure 9 b, c, e, f, h, i) at which marginal bed load transport out of the local scour hole occurred on t_f after the local scour hole got partially refilled by bed load sheet that were transported into the local scour hole. The figure-8 hysteresis loop caused an reworking of infilled sediments so that the

geometrical length scales recovered to sizes comparable to sizes prior to the sediment input (cf. Schlömer & Herget (2021). However, the figure-8 hysteresis loop was not present for the flash flood hydrograph as no refilling of the local scour hole occurred due to the relatively short duration of t_r so that a clockwise hysteresis loop prevailed which highlights the time-dependent nature of local scouring (Figure 9k, l). The two experimental observed hysteresis loops coincide to field observations on local scouring at logs embedded in sand reported by Borg et al., (2007).

The cumulating effects of d_s, l_s, and w_s during subsequent hydrograph events supported working hypothesis (b). However, it becomes obvious that local scouring is an history depended phenomenon for which a relative change in the geometrical length scales during one hydrograph event depends on d_s, l_s, and w_s reached before the occurrence of the event itself as previously described by Tubaldi et al., (2017) and Pizarro and Tubaldi (2019).

The first formative event (i.e. hydrograph I) had the greatest impact on the size of the geometrical length scales, while for $t > 240$ min (i.e. after hydrograph II) the depth incision considerable ceases and slight enlargement in w_s occurred (cf. Schlömer & Herget 2021). The enlargement of w_s is attributed to the convection of detached shear layers from the legs of the HV1 at the lateral sides of the obstacle that result in strong amplification of shear stress at the bed as shown by Kirkil et al. (2008) and Kirkil and Constantinescu (2010).

Although only a simple chronology of hydrographs was considered for which W_k of the individual hydrographs was equal, clear-water conditions prevailed, and limiting boundary conditions (i.e. tilting of the obstacle due local scouring) were neglected, it is speculated that the presence of memory effects (i.e. dependence on antecedent sizes of d_s, l_s, and w_s rather than on actual flow conditions) is generally valid.

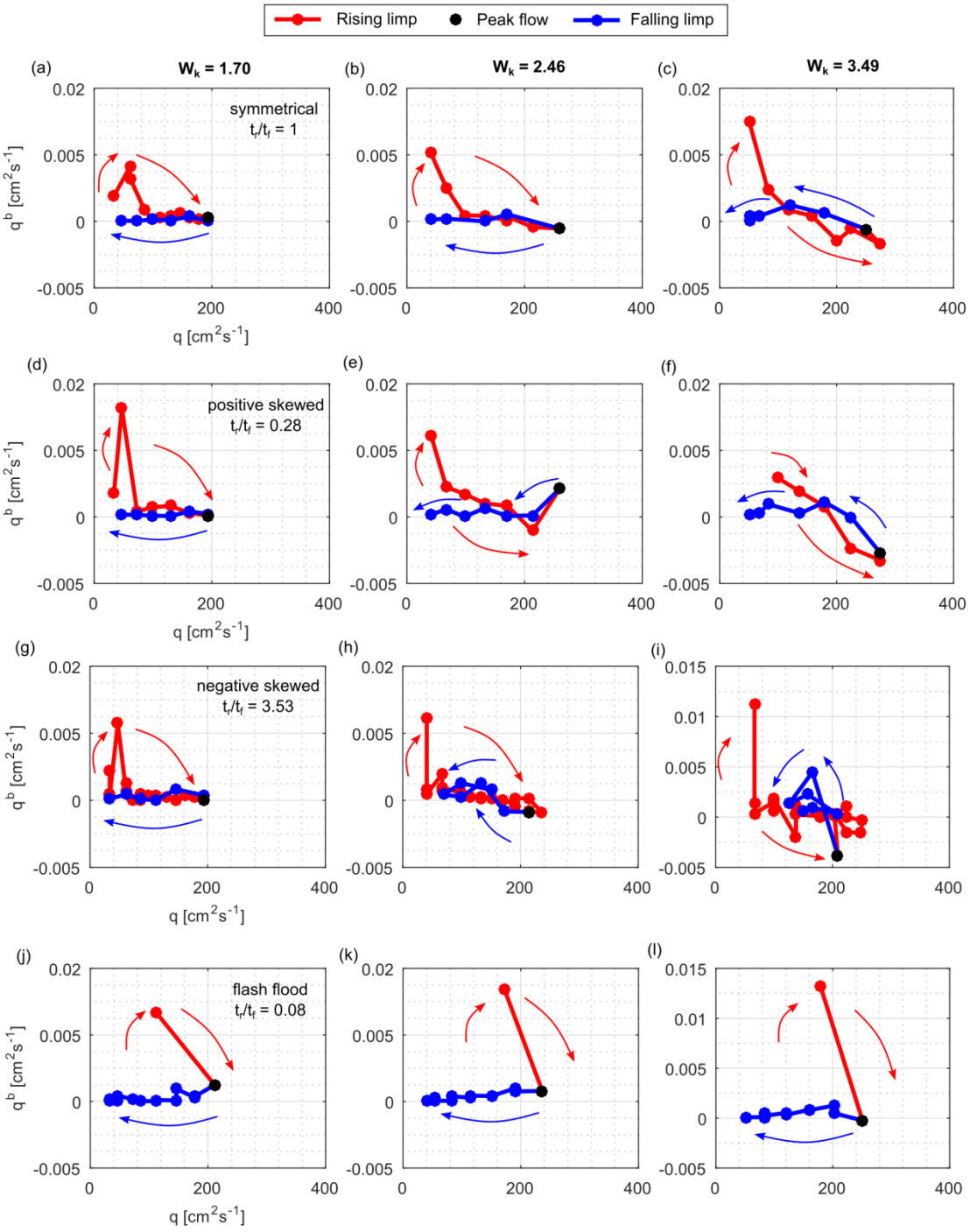
Rising limp
Peak flow
Falling limp
(a)
W_k = 1.70
(b)
W_k = 2.46
(c)
W_k = 3.49
symmetrical
t_r/t_f = 1
positive skewed
t_r/t_f = 0.28
negative skewed
t_r/t_f = 3.53
flash flood
t_r/t_f = 0.08
(d)
(e)
(f)
(g)
(h)
(i)
(j)
(k)
(l)
q^b [cm^2s^{-1}]
q [cm^2s^{-1}]
0.02
0.005
0
-0.005
0.015
0.01
200
400

Figure 9. Hysteresis patterns of bed load transport (q^b) out of the local scour hole for different unit discharge (q) at different total flow work index (W_k)

5. Conclusion

Local scour holes emerging at a boulder-like obstacle exposed to stepped hydrographs of different shape, overall duration, and flow magnitude were physically modelled in a process-focused laboratory flume study. Additionally, local scour holes were exposed to hydrograph chronologies. Recalling the objectives formulated in the Introduction the findings of the present study can be summarized as follows:

1. The enlargement of the frontal scour hole in length and width is triggered by depth incision, steepening of slopes, and gravitational movements at the scour slopes at steady and unsteady discharge. The depth incision is triggered by the HV system that subsides into the local scour hole and causes high bed load transport rates out of the local scour hole at the beginning of local scouring that reduce for later stages of local scouring as the HV expands in diameter which reduces the bed shear stress. For hydrographs this causes hysteresis patterns in bed load transport out of the local scour hole while local scour hole and HV system in time are connected.

   Two mechanistically models are formulated to assess enlargement in local scour length and width based on scour depth, the inclination of frontal scour slopes and the span of the scour hole bottom respectively irrespective of hydraulic boundary conditions (clear-water and live-bed conditions) that can be applied to estimate the spatial extent of countermeasures for local scour protection.

1. Local scouring is history dependent irrespective of hydrograph shape at subsequent hydrograph events. Local scour hole depth, length and width are cumulating in the absence of refilling processes. However, memory effects (i.e. dependence on antecedent sizes of d_s, l_s, and w_s rather than on actual flow conditions) have to be attributed for local scouring at subsequent hydrograph events while the greatest impact on the size of the local scour hole is attributed to the rising limb of the initial hydrograph event for which 80-90 % of the dimensions of scour depth at the end of the experimental series could be observed. The depth incision considerably afterwards due to the connection of form and processes.

   Although the experimental setup has simplified natural complexity it provides insights into the enlargement processes of local scouring at hydrographs that are consistent with prior investigations of the authors for steady discharge. It is furthermore speculated that memory effects are generally valid irrespective of hydraulic conditions of hydrographs. Accounting for memory effects of local scouring is relevant in order to use the geometry of preserved local scour holes at

boulder obstacles located in ephemeral streams as proxy to estimate the minimum duration of the rising limb of a flood hydrograph.

Open Research

The data presented here can be downloaded in tabular form on condition that we are acknowledged in any subsequent publication:

Acknowledgments

The present study was not financially supported.

References

Agisoft (2016): Agisoft PhotoScan User Manual. Professional edition, Version 1.2. https://www.agisoft.com/pdf/photoscan-pro_1_2_en.pdf. Accessed 19 May 2021.

Allen J. R. L. 1984. *Sedimentary structures: Their character and physical basis.* Amsterdam, Elsevier.

Baynes, E R.C., van de Lageweg, W. I., McLelland, S. J., Parsons, D. R., Aberle, J., Dijkstra, J. et al. (2018): Beyond equilibrium: Re-evaluating physical modelling of fluvial systems to represent climate changes. *Earth-Science Reviews* 181, 82–97, https://doi.org/10.1016/j.earscirev.2018.04.007

Bergeron, N. E., & Abrahams, A. D. (1992): Estimating shear velocity and roughness length from velocity profiles. *Water Resources Research* 28 (8), 2155–2158, https://doi.org/10.1029/92WR00897

Bombar, G. (2020): Scour Evolution Around Bridge Piers Under Hydrographs with High Unsteadiness. *Iranian Journal of Science and Technology Transactions of Civil Engineering* 44 (1), 325–337, https://doi.org/10.1007/s40996-019-00321-8

Breusers, H. N. C., & Raudkivi, A. J. (1991): *Scouring* (Hydraulic structures design manual, 2) Rotterdam: Balkema

Brownlie, W. R. (1981): Prediction of flow depth and sediment discharge in open channels, Report KH-R-43A Pasadena: California Institute of Technology

Chang, W.-Y., Lai, J.-S., Yen, C.-L. (2004): Evolution of Scour Depth at Circular Bridge Piers. *Journal of Hydraulic Engineering*130 (9), 905–913, https://doi.org/10.1061/(ASCE)0733-9429(2004)130:9(905)

Chen, Q., Qi, M., Zhong, Q., Li, D. (2017): Experimental study on the multimodal dynamics of the turbulent horseshoe vortex system around a circular cylinder. *Physics of Fluids* 29 (1), 15106, https://doi.org/10.1063/1.4974523

Chreties C., Simarro, G., Teixeira, L. (2008): New Experimental Method to Find Equilibrium Scour at Bridge Piers. Journal of Hydraulic Engineering 134 (10), 1491–1495, https://doi.org/10.1061/(ASCE)0733-9429(2008)134:10(1491)

Chreties C., Teixeira, L., Simarro, G. (2013): Influence of flow conditions on scour hole shape for pier groups. *Proceedings of the Institution of Civil Engineers - Water Management* 166 (3): 111–119, https://doi.org/10.1680/wama.11.00054

Coco, G., & Murray, A. B. (2007): Patterns in the sand: From forcing templates to self-organization. *Geomorphology* 91 (3-4), 271–290, https://doi.org/10.1016/j.geomorph.2007.04.023

Collischonn, W., Fleischmann, A., Paiva, R. C. D., Mejia, A. (2017): Hydraulic Causes for Basin Hydrograph Skewness. *Water Resources Research*53 (12), 10603–10618, https://doi.org/10.1002/2017WR021543

Dargahi, B. (1990): Controlling Mechanism of Local Scouring. *Journal of Hydraulic Engineering*116 (10), 1197–1214, https://doi.org/10.1061/(ASCE)0733-9429(1990)116:10(1197)

Davison A.C., Hinkley D.,V. (2009): *Bootstrap methods and their application*. Cambridge. Cambridge University Press.

Dey, S. (2014): *Fluvial hydrodynamics: Hydrodynamic and sediment transport*. Berlin: Springer.

Escauriaza, C., & Sotiropoulos, F. (2011): Initial stages of erosion and bed form development in a turbulent flow around a cylindrical pier. *Journal of Geophysical Research* 116 (F3), 671, https://doi.org/10.1029/2010JF001749

Ettema R, Melville BW, Barkdoll B. (1998): Scale Effect in Pier-Scour Experiments. Journal of Hydraulic Engineering 124 (6), 639–642, https://doi.org/10.1061/(ASCE)0733-9429(1998)124:6(639)

Ettema, R., Constantinescu, G., Melville, B. (2012): *Evaluation of Bridge Scour Research: Pier Scour Processes and Predictions*. Washington, D.C.: Transportation Research Board.

Euler, Th., Herget, J., Schlömer, O., Benito, G. (2017): Hydromorphological processes at submerged solitary boulder obstacles in streams. *CATENA* 157, 250–267, https://doi.org/10.1016/j.catena.2017.05.028

Gjunsburgs, B., Jaudzems, G., Govša, J. (2010): Hydrograph Shape Impact on the Scour Development with Time at Engineering Structures in River Flow. *Construction Science* 11, 6–12

Hager, W. H., & Hutter, K. (1984): On pseudo-uniform flow in open channel hydraulics. *Acta Mechanica* 53 (3-4), 183–200, https://doi.org/10.1007/BF01177950

Herget, J., Euler, Th., Roggenkamp, Th., Zemke, J. (2013): Obstacle marks as palaeohydraulic indicators of Pleistocene megafloods. *Hydrology Research* 44 (2), 300–317, https://doi.org/10.2166/nh.2012.155

James, M., R., Chandler, J., H., Eltner, A., Fraser, C., Miller, P., E., Mills, J., P., et al. (2019): Guidelines on the use of structure-from-motion photogrammetry

in geomorphic research. Earth Surface Processes and Landforms 44, 20812084, https://doi.org/10.1002/esp.4637

Javernick, J., Brasington, J., Caruso, B. (2014): Modeling the topography of shallow braided rivers using Structure-from-Motion photogrammetry. Geomorphology 213, 166-182, https://doi.org/10.1016/j.geomorph.2014.01.006

Kirkil G., Constantinescu G. (2015): Effects of cylinder Reynolds number on the turbulent horseshoe vortex system and near wake of a surface-mounted circular cylinder. *Physics of Fluids* 27(7), 75102, https://doi.org/10.1063/1.4923063

Kirkil, G., Constantinescu, G. (2010): Flow and turbulence structure around an in-stream rectangular cylinder with scour hole. *Water Resources Research* 46 (11), https://doi.org/10.1029/2010WR009336

Kirkil G., Constantinescu S.G., Ettema R. (2008): Coherent Structures in the Flow Field around a Circular Cylinder with Scour Hole. *Journal of Hydraulic Engineering* 134 (5): 572–587, https://doi.org/10.1061/(ASCE)0733-9429(2008)134:5(572)

Kothyari, U. C., Garde, R. C. J. Kittur G. R. R. (1992): Temporal Variation of Scour Around Circular Bridge Piers. *Journal of Hydraulic Engineering118* (8), 1091–1106, https://doi.org/10.1061/(ASCE)0733-9429(1992)118:8(1091)

Lane, S. N., James, T. D., Crowell, M. D. (2000): Application of digital photogrammetry to complex topography for geomorphological research. Photogrammetric Record 16 (95), 793-821, https://doi.org/10.1111/0031-868X.00152

Lee, S. O., & Sturm, T. W. (2009): Effect of Sediment Size Scaling on Physical Modeling of Bridge Pier Scour. *Journal of Hydraulic Engineering*135 (10), 793–802, https://doi.org/10.1061/(ASCE)HY.1943-7900.0000091

Li, J., Qi, M., Fuhrman, D. R., Chen, Q. (2018): Influence of turbulent horseshoe vortex and associated bed shear stress on sediment transport in front of a cylinder. *Experimental Thermal and Fluid Science* 97, 444–457, https://doi.org/10.1016/j.expthermflusci.2018.05.008

Link, O., Castillo, C., Pizarro, A., Rojas, A., Ettmer, B., Escauriaza, C., Manfreda, S. (2017): A model of bridge pier scour during flood waves. *Journal of Hydraulic Research* 55 (3), 310–323, https://doi.org/10.1080/00221686.2016.1252802

Link, O., González, C., Maldonado, M., Escauriaza, C. (2012): Coherent structure dynamics and sediment particle motion around a cylindrical pier in developing scour holes. *Acta Geophysica.* 60 (6), 1689–1719, https://doi.org/10.2478/s11600-012-0068-y

López, G., Teixeira, L., Ortega-Sánchez, M., Simarro, G. (2014): Estimating Final Scour Depth under Clear-Water Flood Waves. *Journal of Hydraulic Engineering* 140 (3), 328–332, https://doi.org/10.1061/(ASCE)HY.1943-7900.0000804

Manes, C., Coscarella, F., Rogers, A., Gaudio, R. (2018): Viscosity effects on local scour around vertical structures in clear-water conditions. *E3S Web of Conferences*. 40, 3038, https://doi.org/10.1051/e3sconf/20184003038.

Manfreda, S., Link, O., Pizarro, A. (2018): A Theoretically Derived Probability Distribution of Scour. *Water* 10 (11), 1520, https://doi.org/10.3390/w10111520

Mao, L. (2012): The effect of hydrographs on bed load transport and bed sediment spatial arrangement. Journal of Geophysical Research 117 (F3), https://doi.org/10.1029/2012JF002428

Melville, B. W., & Chiew, Y.-M. (1999): Time Scale for Local Scour at Bridge Piers. *Journal of Hydraulic Engineering*125 (1), 59–65, https://doi.org/10.1061/(ASCE)0733-9429(1999)125:1(59)

Melville, B. W., Coleman, S. E. (2000): *Bridge scour*. Highlands Ranch, Colorado: Water Resources Publication.

Morgan J. A., Brogan D., J., Nelson, P. A. (2017): Application of Structure-from-Motion photogrammetry in laboratory flumes. Geomorphology 276, 125–143, https://doi.org/10.1016/j.geomorph.2016.10.021

Nakagawa, H., & Nezu, I. (1993): *Turbulence in Open Channel Flows*, Rotterdam: CRC Press.

Pizarro, A., Manfreda, S., Tubaldi, E. (2020): The Science behind Scour at Bridge Foundations: A Review. *Water* 12 (2), 374, https://doi.org/10.3390/w12020374

Pizarro A., Tubaldi E. (2019): Quantification of Modelling Uncertainties in Bridge Scour Risk Assessment under Multiple Flood Events. *Geosciences* 9 (10), 445, https://doi.org/10.3390/geosciences9100445

Radice, A., Porta, G., Franzetti, S. (2009): Analysis of the time-averaged properties of sediment motion in a local scour process. *Water Resources Research* 45 (3), https://doi.org/10.1029/2007WR006754

Radice, A., & Tran, C. K. (2012): Study of sediment motion in scour hole of a circular pier. *Journal of Hydraulic Research* 50 (1), 44–51, https://doi.org/10.1080/00221686.2011.641764

Richardson, P., D. (1968): The generation of scour marks near obstacles. Journal of Sedimentary Research 38 (4), 965–970, https://doi.org/10.1306/74D71AD7-2B21-11D7-8648000102C1865D

Rodríguez-Iturbe, I., Valdés, J. B. (1979): The geomorphologic structure of hydrologic response. *Water Resources Research* 15 (6), 1409–1420, https://doi.org/10.1029/WR015i006p01409

Rogers, A., Manes, C., Tsuzaki, T. (2020): Measuring the geometry of a developing scour hole in clear-water conditions using underwater sonar scanning. *International Journal of Sediment Research* 35 (1), 105–114, https://doi.org/10.1016/j.ijsrc.2019.07.005

Schlömer, Oliver (2020): Morphodynamic relation of obstacle marks at boulder-like obstructions in time. In *River Flow 2020*. (pp. 719-727) Leiden: CRC Press.

Schlömer, O., Herget, J., Euler, Th. (2020): Boundary condition control of fluvial obstacle mark formation – framework from a geoscientific perspective. Earth Surface Processes and Landforms 45 (1), 189–206, https://doi.org/10.1002/esp.4793

Schlömer, O., Grams, P. E., Buscombe, D., Herget, J. (2021): Geometry of obstacle marks at instream boulders – integration of laboratory investigations and field observations. Earth Surface Processes and Landforms 46 (3), 659679, https://doi.org/10.1002/esp.5055

Schlömer, O. & Herget, J. (2021): Flume experiments on the geometry of local scour holes at boulder-like obstacles during unsteady flow: Part I – Hydrograph Shape and Intensity (submitted to WRR)

Shamloo, H., Rajaratnam, N., Katopodis, C. (2001): Hydraulics of simple habitat structures. Journal of Hydraulic Research 39 (4), 351–366, https://doi.org/10.1080/00221680109499840

Sheppard D. M., Melville B., Demir H. (2014): Evaluation of existing equations for local scour at bridge piers. *Journal of Hydraulic Engineering* 140 (1): 14-23, https://doi.org/10.1061/(ASCE)HY.1943-7900.0000800

Smith, M. W., Carrivick, J., L., Quincey, D. J. (2016): Structure from motion photogrammetry in physical geography. Progress in Physical Geography 40 (2), 247275, https://doi.org/10.1177/0309133315615805

Tabarestani, M. K., Zarrati, A. R. (2017): Local scour calculation around bridge pier during flood event. *KSCE Journal of Civil Engineering* 21 (4), 1462–1472, https://doi.org/10.1007/s12205-016-0986-3

Tregnaghi M., Marion A., Gaudio R. (2007). Affinity and similarity of local scour holes at bed sills. Water Resources Research **43**(11): W11417, https://doi.org/10.1029/2006WR005559

Tubaldi, E., Macorini, L., Izzuddin, B. A., Manes, C., Laio, F. (2017): A framework for probabilistic assessment of clear-water scour around bridge piers. *Structural Safety* 69, 11–22, https://doi.org/10.1016/j.strusafe.2017.07.001

Unger, J., & Hager, W. H. (2007): Down-flow and horseshoe vortex characteristics of sediment embedded bridge piers. *Experiments in Fluids* 42 (1), 1–19, https://doi.org/10.1007/s00348-006-0209-7

Waters, K. A., & Curran, J (2015): Linking bed morphology changes of two sediment mixtures to sediment transport predictions in unsteady flows. *Water Resources Research* 51 (4), 2724–2741, https://doi.org/10.1002/2014WR016083

Wheaton, J. M., Brasington, J., Darby, S. E., Sear, D. A. (2010): Accounting for uncertainty in DEMs from repeat topographic surveys: improved

sediment budgets. *Earth Surface Proceses and Landforms* 35 (2), 136-156, https://doi.org/10.1002/esp.1886

Westoby M.J., Brasington J., Glasser N.F., Hambrey M.J., Reynolds J.M. (2012): 'Structure-from-Motion' photogrammetry: a low-cost, effective tool for geoscience applications. *Geomorphology* 179: 300–314, https://doi.org/10.1016/j.geomorph.2012.08.021.

Williams, G., P. (1989): Sediment concentration versus water discharge during single hydrologic events in rivers. Journal of Hydrology 111 (1-4), 89106, https://doi.org/10.1016/0022-1694(89)90254-0

Williams, P., Balachandar, R., Bolisetti, T. (2019): Examination of Blockage Effects on the Progression of Local Scour around a Circular Cylinder. *Water* 11 (12), 2631, https://doi.org/10.3390/w11122631